Transversal Passivity and Equilibrium Forces in Formation Control

Feng-Yu Yue and Daniel Zelazo

arXiv:2611.15690v1 [eess.SY] 11 Nov 2026

***Abstract*— We consider controller synthesis for distance-constrained formations, aiming to stabilize the target formation manifold while sustaining admissible equilibrium edge forces. Using the newly introduced notion of transversal passivity, we encode the target formation shape, the prescribed edge lengths, and a subspace of internally balanced edge forces as the port target manifolds of the agents and the edge controller. The synthesis task is thereby reformulated as the joint design of a transversally passive edge controller and its output-target subspace. We then propose a general constructive realization of output-strictly transversally passive systems and specialize it to derive a dynamic edge controller that sustains admissible equilibrium edge forces. Through a compatibility analysis across the interconnection, we establish a closed-loop dissipation margin in terms of the controller parameters and prove local convergence of all agent and controller ports to their target manifolds. Numerical simulations validate the results.**

I. Introduction

Distance-constrained formation control has received sustained attention in cooperative control, motivated by broad applications in mobile-robot teams and multi-vehicle coordination [1], [2]. For a group of agents, the objective is to design feedback controllers using relative measurements to achieve prescribed inter-agent distances [2], [3]. Under infinitesimal rigidity, these distance constraints determine the formation shape up to translations and proper rotations, so the admissible target configurations locally form a smooth manifold [4], [5]. Consequently, the control task is naturally formulated as the stabilization of a target formation manifold.

Controller synthesis for this problem must jointly account for the network topology, the agent and controller dynamics, and the nonlinearities induced by the geometric distance constraints. Passivity provides a powerful modular framework for this task by decoupling the component dynamics from the network interconnection, thereby enabling constructive edge-controller synthesis [6], [7]. Existing passivity-based approaches accommodate formation geometry by steering relative edge outputs to prescribed compact target sets [6] or by shaping distance-error potentials [8]. Beyond passivity, edge-space formulations reduce local stability to spectral properties of a linearized edge operator and enable synthesis of stabilizing edge gains via semidefinite programming [9].

However, in all of these error-driven constructions, the equilibrium edge forces are not treated as a design freedom: the edge dynamics require every edge force to vanish once the distance errors reach zero. In fact, edge forces need not vanish individually at equilibrium, since internally balanced edge forces (corresponding to *self-stresses*) can remain nonzero without disturbing the agents. Sustaining such internal forces plays a key role in enhancing structural stiffness [10] and maintaining internal tension [11]. This motivates developing a passivity-based edge-controller synthesis where the admissible space of equilibrium edge forces can be explicitly prescribed.

To address this synthesis problem, our recently introduced notion of *transversal passivity* [12] provides a natural framework. It formulates dissipation relative to prescribed input and output target manifolds while retaining the modularity of classical passivity in decoupling network topology from system dynamics. In the formation-control interconnection, this allows us to encode the rigid-motion orbit of the target shape as the agent output manifold and the prescribed edge lengths as the controller input manifold, while specifying a subspace of internally balanced edge forces as the controller output target. Consequently, the control task is reformulated as the joint design of a transversally passive edge controller and its output-target subspace to achieve shape convergence while sustaining desired equilibrium edge forces.

In this paper, we study the distance-constrained formation controller synthesis problem while sustaining admissible equilibrium edge forces. Our main contributions are as follows. First, we reformulate the considered formation control task as the joint design of a transversally passive edge controller and its output-target subspace. Second, for a smooth input target manifold and a linear output target subspace, we propose a constructive realization of output-strictly transversally passive systems, which specializes to a dynamic edge controller parameterized by the output-target subspace to sustain the corresponding equilibrium forces. Third, through a compatibility analysis under transversal passivity, we establish a closed-loop dissipation margin in terms of the controller parameters and prove local convergence of all agent and controller ports to their target manifolds, thereby achieving the desired formation with equilibrium forces in the prescribed subspace. Although sustaining nonzero equilibrium forces generally leads to a centralized implementation, our numerical simulations validate the theoretical results and demonstrate how a localized subspace choice can preserve these forces with sparser subgraph-confined coupling.

The remainder of this paper is organized as follows. Section II reviews transversal passivity and distance-constrained formation control. Section III reformulates the formation control problem within the transversal passivity framework, followed by the constructive controller synthesis and local

This work was supported by the Israel Science Foundation grant no. 453/24. Feng-Yu Yue and Daniel Zelazo are with the Stephen B. Klein Faculty of Aerospace Engineering, Technion – Israel Institute of Technology, Haifa 3200003, Israel. Emails: *fengyu.yue@campus.technion.ac.il*, *dzelazo@technion.ac.il.*

convergence analysis in Section IV. Numerical simulations and concluding remarks are given in Sections V and VI, respectively.

Notations: All inner products $\langle\cdot,\cdot\rangle$ and norms $\|\cdot\|$ are Euclidean. We denote by I_n the $n\times n$ identity matrix, by $\mathbf{1}_n\in\mathbb{R}^n$ the all-ones vector, by $\otimes$ the Kronecker product, and by $SO(2)$ the group of 2×2 proper rotation matrices.

For a set $\mathcal{S}$, $|\mathcal{S}|$ denotes its cardinality, and $\operatorname{dist}(x,\mathcal{S}):=\inf_{y\in\mathcal{S}}\|x-y\|$ denotes the Euclidean distance from $x\in\mathbb{R}^n$ to a nonempty $\mathcal{S}\subseteq\mathbb{R}^n$. For a linear subspace $\mathcal{L}\subseteq\mathbb{R}^n$, $\mathrm{P}_{\mathcal{L}}$ and $\mathrm{P}_{\mathcal{L}^\perp}=I_n-\mathrm{P}_{\mathcal{L}}$ denote the orthogonal projectors onto $\mathcal{L}$ and its orthogonal complement $\mathcal{L}^\perp$, respectively. For a smooth manifold $\mathcal{M}\subseteq\mathbb{R}^n$, $T_p\mathcal{M}$ and $N_p\mathcal{M}$ denote its tangent and normal spaces at $p\in\mathcal{M}$, respectively.

An undirected graph $\mathcal{G}=(\mathcal{V},\mathcal{E})$ consists of a finite vertex set $\mathcal{V}$ and an edge set $\mathcal{E}\subseteq\mathcal{V}\times\mathcal{V}$. Assigning an arbitrary orientation to each edge $e_k\in\mathcal{E}$, the incidence matrix $E\in\mathbb{R}^{|\mathcal{V}|\times|\mathcal{E}|}$ is defined entrywise by $[E]_{ik}:=1$ if vertex i is the head of e_k, $[E]_{ik}:=-1$ if i is the tail of e_k, and $[E]_{ik}:=0$ otherwise.

II. Preliminaries

This section introduces necessary background on transversal passivity and the distance-constrained formation control.

A. Transversal Passivity

Consider two nonlinear systems

$$\Sigma_i:\quad \dot{x}_i=f_i(x_i,u_i),\quad y_i=h_i(x_i,u_i),\qquad i=1,2,$$

with state $x_i\in\mathcal{X}_i\subseteq\mathbb{R}^{n_i}$, input $u_i\in\mathcal{U}_i\subseteq\mathbb{R}^{m_i}$, and output $y_i\in\mathcal{Y}_i\subseteq\mathbb{R}^{m_i}$, where $\mathcal{X}_i,\mathcal{U}_i,\mathcal{Y}_i$ are open, f_i is locally Lipschitz, and h_i is C^1. The two systems are interconnected via the power-conserving linear feedback law

$$u_1=-\Gamma^\top y_2,\qquad u_2=\Gamma y_1, \tag{1}$$

where $\Gamma\in\mathbb{R}^{m_2\times m_1}$ is the *forward channel* and $-\Gamma^\top$ is the *reverse channel*.

Equip each Σ_i with embedded target submanifolds $\mathcal{M}_{u_i}\subseteq\mathcal{U}_i$ and $\mathcal{M}_{y_i}\subseteq\mathcal{Y}_i$. On tubular neighborhoods $\mathcal{N}_{u_i}\subseteq\mathcal{U}_i$ and $\mathcal{N}_{y_i}\subseteq\mathcal{Y}_i$ where the Euclidean nearest-point projections $r_{u_i}:\mathcal{N}_{u_i}\to\mathcal{M}_{u_i}$ and $r_{y_i}:\mathcal{N}_{y_i}\to\mathcal{M}_{y_i}$ are uniquely defined and smooth, the *transverse port error maps* are defined as

$$e_{u_i}(u_i):=u_i-r_{u_i}(u_i),\qquad e_{y_i}(y_i):=y_i-r_{y_i}(y_i), \tag{2}$$

These error maps represent the normal displacements from the targets and satisfy $\|e_{u_i}(u_i)\|=\operatorname{dist}(u_i,\mathcal{M}_{u_i})$ and $\|e_{y_i}(y_i)\|=\operatorname{dist}(y_i,\mathcal{M}_{y_i})$. Define the tubular domain $\mathcal{D}_i:=\{(x_i,u_i)\in\mathcal{X}_i\times\mathcal{N}_{u_i}:h_i(x_i,u_i)\in\mathcal{N}_{y_i}\}$.

Definition 1 (Transversal passivity [12]): The system Σ_i is called $(\mathcal{M}_{u_i},\mathcal{M}_{y_i})$*-passive* on $\mathcal{D}_i\neq\emptyset$ if there exist a continuously differentiable storage function $V_i:\mathcal{X}_i\to\mathbb{R}_{\geq 0}$ and constants $\varepsilon_i,\gamma_i\geq 0$ such that, for all $(x_i,u_i)\in\mathcal{D}_i$,

$$\dot{V}_i(x_i,u_i)\leq\langle e_{u_i}(u_i),e_{y_i}(y_i)\rangle-\varepsilon_i\|e_{y_i}(y_i)\|^2-\gamma_i\|e_{u_i}(u_i)\|^2.$$

Σ_i is *output-strictly* $(\mathcal{M}_{u_i},\mathcal{M}_{y_i})$-passive if $\varepsilon_i>0$.

Transversal passivity penalizes only deviations normal to $(\mathcal{M}_{u_i},\mathcal{M}_{y_i})$ while leaving motions along the target manifolds unpenalized.

Suppose now that both subsystems Σ_i in (1) are $(\mathcal{M}_{u_i},\mathcal{M}_{y_i})$-passive with storage functions $V_i(x_i)$ and constants $\varepsilon_i,\gamma_i\geq 0$. Although (1) is power-conserving ($\langle u_1,y_1\rangle+\langle u_2,y_2\rangle=0$), this cancellation generally fails under transversal passivity because the supply rates are evaluated at the transverse port errors rather than the port signals. To quantify this mismatch for the forward channel Γ, we define the *compatibility defect* [12, Definitions 2–3]

$$\delta_{\mathrm{fc}}(y_1):=e_{u_2}(\Gamma y_1)-\Gamma\,e_{y_1}(y_1)=\Gamma\,r_{y_1}(y_1)-r_{u_2}(\Gamma y_1),$$

which measures the failure of Γ to commute with the nearest-point projections. The forward channel Γ is called *exactly compatible* on a set $\mathcal{S}$ if $\delta_{\mathrm{fc}}(y_1)=0$ for all $y_1\in\mathcal{S}$, and *first-order compatible* along $\mathcal{S}$ if $\delta_{\mathrm{fc}}(y_1)=0$ and $\mathrm{d}_{y_1}\delta_{\mathrm{fc}}=0$ for all $y_1\in\mathcal{S}$. The defect $\delta_{\mathrm{rc}}(y_2)$ and compatibility notions for the reverse channel $-\Gamma^\top$ are defined analogously.

For the feedback interconnection (1) with composite storage $V_{\mathrm{cl}}(x):=V_1(x_1)+V_2(x_2)$ and $x=(x_1,x_2)$, the closed-loop dissipation satisfies [12, Theorem 1] $\dot{V}_{\mathrm{cl}}(x)\leq s_\delta(x)-W_0(x)$, where $W_0(x)$ collects the subsystem dissipation and

$$s_\delta(x):=\langle\delta_{\mathrm{rc}}(y_2(x)),e_{y_1}(y_1(x))\rangle+\langle\delta_{\mathrm{fc}}(y_1(x)),e_{y_2}(y_2(x))\rangle$$

is the *residual transverse supply*. Since e_{y_i}, δ_{fc}, and δ_{rc} vanish when all ports lie on their target manifolds, s_δ is locally at least quadratic, yielding three regimes: (i) *vanishing residual* ($s_\delta\equiv 0$), ensured if both channels are exactly compatible; (ii) *quadratic cancellation* (s_δ is locally cubic), ensured if both channels are first-order compatible; and (iii) *nonzero quadratic residual*, where W_0 must dominate s_δ at second order for net dissipation. Combined with compact confinement, port convergence guarantees across these three regimes are established in [12, Corollary 2, Theorems 2 and 3].

B. Graph Rigidity and Distance-Constrained Formations

Consider $n\geq 3$ single-integrator agents in $\mathbb{R}^2$ with dynamics $\dot{p}_i=u_i$, where $p_i,u_i\in\mathbb{R}^2$ denote the position and control input of agent $i\in\mathcal{V}$. The inter-agent interaction topology is modeled by a connected undirected graph $\mathcal{G}=(\mathcal{V},\mathcal{E})$ with $|\mathcal{E}|=m$ edges. The formation is represented by a *framework* $(\mathcal{G},p)$, where $p=(p_1^\top,\dots,p_n^\top)^\top\in\mathbb{R}^{2n}$ is the configuration of the agents, yielding $\dot{p}=u$. Let $\bar{E}:=E\otimes I_2\in\mathbb{R}^{2n\times 2m}$, so that the k-th block $(\bar{E}^\top p)_k=p_i-p_j$ gives the relative position of edge $e_k=(i,j)\in\mathcal{E}$.

The shape of $(\mathcal{G},p)$ is described by the *rigidity function*

$$\mathrm{r}_{\mathcal{G}}(p)=\frac{1}{2}(\|(\bar{E}^\top p)_1\|^2,\dots,\|(\bar{E}^\top p)_m\|^2)^\top\in\mathbb{R}^m,$$

with

$$R_{\mathcal{G}}(p):=\frac{\partial\mathrm{r}_{\mathcal{G}}}{\partial p}(p)=\operatorname{blkdiag}((\bar{E}^\top p)_1^\top,\dots,(\bar{E}^\top p)_m^\top)\bar{E}^\top$$

being the *rigidity matrix*. For a framework $(\mathcal{G},p)$, a *stress* is a vector of scalars $\omega=(\omega_1,\dots,\omega_m)^\top\in\mathbb{R}^m$ assigned to the edges. A stress is called a *self-stress* if the induced edge

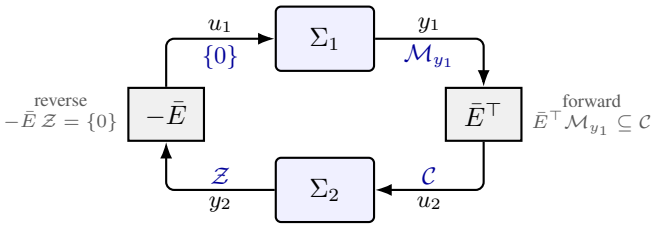


Fig. 1: Feedback interconnection of the agents Σ_1 and the edge controller Σ_2 through the forward channel $\bar{E}^\top$ and the reverse channel $-\bar{E}$. Each port signal is annotated with its target manifold (blue); the channel annotations relate the targets across the interconnection.

forces $\big(\omega_1(\bar{E}^\top p)_1^\top, \dots, \omega_m(\bar{E}^\top p)_m^\top\big)^\top \in \mathbb{R}^{2m}$ are balanced at every node, i.e.,

$$\bar{E}\big(\omega_1(\bar{E}^\top p)_1^\top, \dots, \omega_m(\bar{E}^\top p)_m^\top\big)^\top = R_{\mathcal{G}}(p)^\top \omega = 0. \quad (3)$$

Thus, $\ker(R_{\mathcal{G}}(p)^\top)$ is the space of self-stresses of $(\mathcal{G}, p)$ [13], [14].

Let $p^\star \in \mathbb{R}^{2n}$ be a target configuration with desired edge lengths $d = (d_1, \dots, d_m)^\top$, where $d_k = \|(\bar{E}^\top p^\star)_k\| > 0$ for all $e_k \in \mathcal{E}$. Throughout this paper, we assume that the target framework $(\mathcal{G}, p^\star)$ is *infinitesimally rigid*, meaning that $\operatorname{rank}(R_{\mathcal{G}}(p^\star)) = 2n - 3$ [4], [15]. In this case, $\dim\ker(R_{\mathcal{G}}(p^\star)^\top) = m-(2n-3)$, and the only infinitesimal motions at $p^\star$ that preserve the edge lengths are planar translations and rotations. The control objective is to design the control input u such that the agents locally converge to the target formation matching $p^\star$ up to planar translations and proper rotations, while sustaining desired edge forces at equilibrium.

III. Problem Reformulation via Transversal Passivity

This section reformulates the distance-constrained formation control problem within the transversal passivity framework [12]. Whereas classical passivity measures the supply $\langle u, y\rangle$ relative to the origin to certify convergence to a point equilibrium, the agent positions here must converge to the noncompact manifold of configurations with the desired shape. Transversal passivity accommodates this objective by evaluating the supply $\langle e_u, e_y\rangle$ via the transverse port errors (2) relative to prescribed *target manifolds*. The design thus begins by encoding the control objective as agent target manifolds, from which consistent controller targets follow through the interconnection channels.

A. Feedback Interconnection with Edge Ports

Consider the feedback interconnection in Fig. 1, where the plant Σ_1 represents the stacked agent dynamics with input $u_1 := u$ and output $y_1 := p$,

$$\Sigma_1: \quad \dot{p} = u_1, \qquad y_1 = p, \quad (4)$$

and Σ_2 is the edge controller to be designed. Choosing the forward channel $\bar{E}^\top$ and reverse channel $-\bar{E}$ yields the edge relative positions $u_2 = \bar{E}^\top p$ and plant input $u_1 = -\bar{E}y_2$.

B. Agent Target Manifolds

The targets of Σ_1 are dictated by the control objective rather than chosen. First, at steady state the agents should be at rest, so the input target is

$$\mathcal{M}_{u_1} = \{0\}. \quad (5)$$

Second, the agent positions should form the desired shape. Since the edge lengths determine $p^\star$ only up to planar translations and rotations, the output target cannot be a single point. Instead, we take the orbit of $p^\star$ under planar rigid motions,

$$\mathcal{M}_{y_1} = \big\{(I_n \otimes Q)p^\star + \mathbf{1}_n \otimes \eta : Q \in SO(2),\ \eta \in \mathbb{R}^2\big\}. \quad (6)$$

Since $d_k > 0$, the only planar rigid motion fixing $p^\star$ is the identity, and $SE(2)$ acts properly on $\mathbb{R}^{2n}$. Therefore, $\mathcal{M}_{y_1}$ is a connected, closed, embedded three-dimensional submanifold of $\mathbb{R}^{2n}$ diffeomorphic to $SE(2)$ [16]. Moreover, by infinitesimal rigidity, $\mathcal{M}_{y_1}$ coincides near $p^\star$ with the set of configurations satisfying all distance constraints, while excluding reflections and other incongruent realizations of the same distances.

Since $\mathcal{M}_{y_1}$ is a closed embedded submanifold, it admits a tubular neighborhood $\mathcal{N}_{y_1} \subseteq \mathbb{R}^{2n}$ on which the nearest-point projection r_{y_1} is well defined and smooth, with transverse error $e_{y_1}(p) = p - r_{y_1}(p)$. On the input side, we take $\mathcal{N}_{u_1} = \mathbb{R}^{2n}$, $r_{u_1} \equiv 0$, and $e_{u_1}(u_1) = u_1$. Choosing the output-distance storage function

$$V_1(p) = \frac{1}{2}\operatorname{dist}(p, \mathcal{M}_{y_1})^2 = \frac{1}{2}\|e_{y_1}(p)\|^2 \quad (7)$$

and differentiating V_1 along Σ_1 yields $\dot{V}_1 = \langle e_{y_1}(p), u_1\rangle = \langle e_{u_1}(u_1), e_{y_1}(y_1)\rangle$. Thus, Σ_1 is $(\{0\}, \mathcal{M}_{y_1})$-passive on $\mathcal{N}_{y_1} \times \mathbb{R}^{2n}$ [12, Proposition 2]. Note that r_{y_1} is an analysis tool and is not computed by the agents.

C. Controller Target Manifolds

In contrast to the agent targets, the controller targets are design choices, constrained only by consistency with the agent targets through the interconnection channels. At the input port, each edge attains its desired length d_k if and only if $u_{2,k} \in d_k S^1 := \{x \in \mathbb{R}^2 : \|x\| = d_k\}$. At the output port, since $u_1 = -\bar{E}y_2$, the constraint $\mathcal{M}_{u_1} = \{0\}$ requires the target outputs to lie in $\ker \bar{E}$, which by (3) also contains the edge forces induced by any self-stress $\omega \in \ker(R_{\mathcal{G}}(p)^\top)$. Accordingly, we choose the controller target manifolds as

$$\mathcal{M}_{u_2} = \mathcal{C} := \prod_{k=1}^{m} d_k S^1, \qquad \mathcal{M}_{y_2} = \mathcal{Z} \subseteq \ker \bar{E}. \quad (8)$$

We choose $\mathcal{C}$ rather than the realizable image $\bar{E}^\top \mathcal{M}_{y_1} = \{(I_m \otimes Q)\bar{E}^\top p^\star : Q \in SO(2)\}$ as the controller input target because its nearest-point projection is edgewise: projecting onto $\mathcal{C}$ only rescales each $u_{2,k}$ to length d_k (Fig. 2), whereas projecting onto $\bar{E}^\top \mathcal{M}_{y_1}$ requires fitting a common rotation to all edges simultaneously. This relaxation introduces no spurious targets: since infinitesimal rigidity implies local rigidity [13], $\mathcal{C} \cap \operatorname{range} \bar{E}^\top = \bar{E}^\top \mathcal{M}_{y_1}$ in a neighborhood

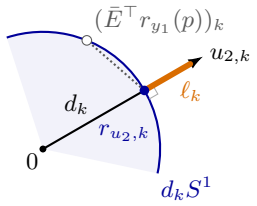


Fig. 2: Edgewise projection onto $\mathcal{C}$ for edge k. The nearest point $r_{u_2,k} = d_k \widehat{u}_{2,k}$ on the target circle $d_k S^1$ (blue) is obtained by rescaling $u_{2,k}$, and the transverse error $e_{u_2,k} = \ell_k \widehat{u}_{2,k}$ (orange) is normal to the circle. The hollow point is the k-th edge of the nearest target formation $r_{y_1}(p)$; the dotted chord to it is the forward compatibility defect analyzed in Section IV.

of $\bar{E}^\top \mathcal{M}_{y_1}$. Meanwhile, the linear subspace $\mathcal{Z} \subseteq \ker \bar{E}$ is selected to prescribe the admissible balanced edge forces at equilibrium.

For Σ_2, the edgewise projection onto $\mathcal{C}$ is smooth on $\mathcal{N}_{u_2} := \{u_2 \in \mathbb{R}^{2m} : u_{2,k} \neq 0,\ \forall k \in \{1,\dots,m\}\}$, while for the linear subspace $\mathcal{Z} \subseteq \ker \bar{E}$ the nearest-point projection is the orthogonal projector $\mathrm{P}_{\mathcal{Z}}$, which is defined globally, i.e., $\mathcal{N}_{y_2} = \mathbb{R}^{2m}$. On $\mathcal{N}_{u_2}$, define the edge-length error $\ell_k := \|u_{2,k}\| - d_k$ and unit direction $\widehat{u}_{2,k} := u_{2,k}/\|u_{2,k}\|$, and stack them as $\ell := (\ell_1,\dots,\ell_m)^\top$, and

$$U(u_2) := \mathrm{blkdiag}(\widehat{u}_{2,1},\dots,\widehat{u}_{2,m}), \tag{9}$$

which satisfies $U(u_2)^\top U(u_2) = I_m$. The port projections and transverse errors of Σ_2 are then given by

$$\begin{aligned} r_{u_2}(u_2) &= U(u_2)d, \quad e_{u_2}(u_2) = U(u_2)\ell, \\ r_{y_2}(y_2) &= \mathrm{P}_{\mathcal{Z}}\, y_2, \qquad e_{y_2}(y_2) = \mathrm{P}_{\mathcal{Z}^\perp}\, y_2, \end{aligned} \tag{10}$$

with $\|e_{u_2}(u_2)\| = \|\ell\|$.

D. Problem Formulation

At this point, the agent side of the interconnection is fully specified: Σ_1 is $(\{0\}, \mathcal{M}_{y_1})$-passive, and the controller input target is fixed as $\mathcal{M}_{u_2} = \mathcal{C}$. What remains is the edge controller Σ_2 together with its output target $\mathcal{Z}$, which must be chosen jointly. The formation control task thus reduces to the following synthesis problem.

Problem 1: Select a linear output-target subspace $\mathcal{M}_{y_2} = \mathcal{Z} \subseteq \ker \bar{E}$ and synthesize a dynamic edge controller Σ_2 such that:

i) Σ_2 is output-strictly $(\mathcal{C}, \mathcal{Z})$-passive;
ii) at any target configuration $p \in \mathcal{M}_{y_1}$, the closed-loop equilibria sustain the balanced edge forces $y_2 \in \mathcal{Z}$ induced by the corresponding self-stresses in $\ker(R_{\mathcal{G}}(p)^\top)$; and
iii) the closed-loop system achieves local convergence, with all realized port signals (u_1, y_1, u_2, y_2) converging to $(\mathcal{M}_{u_1}, \mathcal{M}_{y_1}, \mathcal{C}, \mathcal{Z})$.

Two features distinguish Problem 1 from a standard passivity-based interconnection. First, since $\mathcal{C}$ relaxes $\bar{E}^\top \mathcal{M}_{y_1}$, projecting onto the targets does not commute with the forward channel, i.e., the interconnection carries a nonzero compatibility defect, so the general interconnection results of [12] do not apply directly. Second, the choice of $\mathcal{Z}$ governs both the equilibrium edge forces sustained and the inter-edge coupling of the controller, with the two extremes $\mathcal{Z} = \{0\}$ and $\mathcal{Z} = \ker \bar{E}$ trading one against the other.

Section IV addresses Problem 1: for a given $\mathcal{Z}$, it constructs an output-strictly transversally passive edge controller (Proposition 1), shows that the compatibility defect enters the closed-loop energy balance only at second order (Proposition 2 and Lemma 1), establishes local convergence (Theorem 1), and examines how the choice of $\mathcal{Z}$ trades off retained equilibrium forces against inter-edge coupling. Section V then compares decoupled, centralized, and localized choices of $\mathcal{Z}$ numerically.

IV. Constructive Controller Synthesis and Local Convergence

In this section, we address Problem 1 for a given subspace $\mathcal{Z} \subseteq \ker \bar{E}$. We synthesize an output-strictly $(\mathcal{M}_{u_2}, \mathcal{M}_{y_2})$-passive dynamical controller Σ_2 and establish local closed-loop port convergence. For brevity, the arguments of $e_{u_2}(u_2)$, $e_{y_2}(y_2)$ and $U(u_2)$ are omitted when they are clear from the context.

A. Construction from the Transverse Supply

We first present a general construction of output-strictly transversally passive systems for an arbitrary smooth input target manifold $\mathcal{M}_u$ (with transverse error e_u on $\mathcal{N}_u$) and a linear output target subspace $\mathcal{M}_y$ (with $e_y = \mathrm{P}_{\mathcal{M}_y^\perp} y$).

Starting from the transverse supply $\langle e_u, e_y \rangle$, we seek state dynamics and an output map satisfying the output-strict dissipation inequality

$$\dot{V} \leq \langle e_u, e_y \rangle - \varepsilon \|e_y\|^2,$$

with $\varepsilon > 0$. For a state-only storage function $V(\xi)$, we have $\dot{V} = \langle \nabla V(\xi), \dot{\xi} \rangle$, whereas the linearity of $\mathcal{M}_y$ gives $\langle e_u, e_y \rangle = \langle \mathrm{P}_{\mathcal{M}_y^\perp} e_u, y \rangle$. This suggests the classical port-Hamiltonian structure [17], [18]: taking V as the Hamiltonian, we introduce a matrix-valued design map $L(u)$ from the state space to the output space, drive ξ by the projected transverse input error through $L(u)^\top$, and take the collocated output $L(u)\nabla V(\xi)$, complemented by damping and a direct feedthrough of e_u. This leads to the following result.

Proposition 1 (Constructive transversal passivity realization): Let $V : \mathcal{X} \to \mathbb{R}_{\geq 0}$ be C^2 on an open state domain $\mathcal{X} \subseteq \mathbb{R}^{n_\xi}$, and let $L(u)$ be a C^1 matrix-valued map of compatible dimensions on $\mathcal{N}_u$. For any gains $a, b, g > 0$ and any linear subspace $\mathcal{M}_y$, the system

$$\begin{cases} \dot{\xi} = L(u)^\top \mathrm{P}_{\mathcal{M}_y^\perp} \big(b\, e_u - a\, L(u) \nabla V(\xi) \big), \\ y = b\, L(u) \nabla V(\xi) + g\, e_u, \end{cases} \tag{11}$$

is output-strictly $(\mathcal{M}_u, \mathcal{M}_y)$-passive on $\mathcal{X} \times \mathcal{N}_u$ with storage function $V(\xi)$, satisfying

$$\begin{aligned} \dot{V} &= \langle e_u, e_y \rangle - a \|\mathrm{P}_{\mathcal{M}_y^\perp} L \nabla V\|^2 - g \|\mathrm{P}_{\mathcal{M}_y^\perp} e_u\|^2 \\ &\leq \langle e_u, e_y \rangle - \frac{a}{b^2 + ag} \|e_y\|^2. \end{aligned} \tag{12}$$

Moreover, at any held target input $u \in \mathcal{M}_u$, a state $\xi \in \mathcal{X}$ is an equilibrium of (11) if and only if $L(u)\nabla V(\xi) \in \mathcal{M}_y$.

Proof: By (11), $e_y = \mathrm{P}_{\mathcal{M}_y^\perp} y = b\,\mathrm{P}_{\mathcal{M}_y^\perp} L\nabla V + g\,\mathrm{P}_{\mathcal{M}_y^\perp} e_u$. Differentiating V along (11) and substituting $b\,\mathrm{P}_{\mathcal{M}_y^\perp} L\nabla V = e_y - g\,\mathrm{P}_{\mathcal{M}_y^\perp} e_u$ into $\dot V = \nabla V^\top \dot\xi$ yields the equality in (12). Applying the Cauchy–Schwarz inequality gives

$$\|e_y\|^2 \le \left(\frac{b^2}{a} + g\right)\left(a\|\mathrm{P}_{\mathcal{M}_y^\perp} L\nabla V\|^2 + g\|\mathrm{P}_{\mathcal{M}_y^\perp} e_u\|^2\right),$$

which, together with the triangle inequality $\|e_y\| \le b\|\mathrm{P}_{\mathcal{M}_y^\perp} L\nabla V\| + g\|\mathrm{P}_{\mathcal{M}_y^\perp} e_u\|$, establishes the inequality in (12). Finally, when $u \in \mathcal{M}_u$, we have $e_u = 0$ and $\dot\xi = -a\,L^\top \mathrm{P}_{\mathcal{M}_y^\perp} L\nabla V$. Taking the inner product with ∇V gives $\langle \nabla V, \dot\xi\rangle = -a\|\mathrm{P}_{\mathcal{M}_y^\perp} L\nabla V\|^2$. Hence, $\dot\xi = 0$ if and only if $\mathrm{P}_{\mathcal{M}_y^\perp} L\nabla V = 0$. ∎

The projector $\mathrm{P}_{\mathcal{M}_y^\perp}$ in the state dynamics of (11) is essential: state directions with $L(u)\nabla V(\xi) \in \mathcal{M}_y$ are neither driven by e_u nor damped, so the system can hold a nonzero state at equilibrium while its output remains on the target $\mathcal{M}_y$. In the formation control setting, these directions sustain the nonzero equilibrium edge forces in $\mathcal{Z}$.

B. Edge Controller and Target Equilibria

To address Problem 1, we specialize Proposition 1 to the edge controller Σ_2 with port targets $(\mathcal{M}_{u_2}, \mathcal{M}_{y_2}) = (\mathcal{C}, \mathcal{Z})$. To generate radial edge forces, we assign one scalar state $\xi_k \in \mathbb{R}$ to each edge $e_k \in \mathcal{E}$, stacked as $\xi \in \mathbb{R}^m$, with quadratic storage $V_2(\xi) = \frac{1}{2}\|\xi\|^2$, and choose $L(u_2) = U(u_2)$ to align each ξ_k with the unit edge direction $\widehat{u}_{2,k}$. With $e_{u_2}(u_2) = U(u_2)\ell$ from (10), the realization (11) yields the output-strictly $(\mathcal{C}, \mathcal{Z})$-passive edge controller

$$\Sigma_2 : \quad \begin{cases} \dot\xi = U(u_2)^\top \mathrm{P}_{\mathcal{Z}^\perp} U(u_2)\,\big(b\,\ell - a\,\xi\big), \\ y_2 = U(u_2)\,\big(b\,\xi + g\,\ell\big). \end{cases} \tag{13}$$

Componentwise, edge e_k outputs the radial force $y_{2,k} = \widehat{u}_{2,k}(b\,\xi_k + g\,\ell_k)$, and its state evolves as

$$\dot\xi_k = \widehat{u}_{2,k}^\top \sum_{j=1}^{m} [\mathrm{P}_{\mathcal{Z}^\perp}]_{kj}\, \widehat{u}_{2,j}\,(b\,\ell_j - a\,\xi_j), \tag{14}$$

where $[\mathrm{P}_{\mathcal{Z}^\perp}]_{kj} \in \mathbb{R}^{2\times 2}$ denotes the (k,j) block of $\mathrm{P}_{\mathcal{Z}^\perp}$. Hence, edge e_k requires $\widehat{u}_{2,j}$, ℓ_j, and ξ_j only from the edges e_j with $[\mathrm{P}_{\mathcal{Z}^\perp}]_{kj} \neq 0$, so the block sparsity of $\mathrm{P}_{\mathcal{Z}^\perp}$ determines the inter-edge coupling pattern. For $\mathcal{Z} = \mathcal{Z}_0 \otimes \mathbb{R}^2$ with $\mathcal{Z}_0 \subseteq \mathbb{R}^m$, we have $\mathrm{P}_{\mathcal{Z}^\perp} = \mathrm{P}_{\mathcal{Z}_0^\perp} \otimes I_2$, and (14) reduces to $\dot\xi_k = \sum_j [\mathrm{P}_{\mathcal{Z}_0^\perp}]_{kj}\,(\widehat{u}_{2,k}^\top \widehat{u}_{2,j})(b\,\ell_j - a\,\xi_j)$, which involves only the relative orientations of the edges.

Interconnecting Σ_1 and Σ_2 via Fig. 1 (with U, ℓ, and e_{u_2} evaluated at $u_2 = \bar E^\top p \in \mathcal{N}_{u_2}$) and defining the normalized rigidity matrix and controller Gram matrix

$$R(p) := U(\bar E^\top p)^\top \bar E^\top,\; G_{\mathcal{Z}}(p) := U(\bar E^\top p)^\top \mathrm{P}_{\mathcal{Z}^\perp} U(\bar E^\top p),$$

we obtain the closed-loop dynamics

$$\begin{cases} \dot p = -R(p)^\top \big(b\,\xi + g\,\ell\big), \\ \dot\xi = G_{\mathcal{Z}}(p)\big(b\,\ell - a\,\xi\big). \end{cases} \tag{15}$$

Since $R_{\mathcal{G}}(p) = \mathrm{diag}\big(\|(\bar E^\top p)_1\|, \dots, \|(\bar E^\top p)_m\|\big) R(p)$, infinitesimal rigidity implies $\ker R(p) = T_p\mathcal{M}_{y_1}$ and $\operatorname{rank} R(p) = 2n-3$ for all $p \in \mathcal{M}_{y_1}$.

We next characterize the closed-loop equilibria on $\mathcal{M}_{y_1}$ and the sustained equilibrium edge forces. For any p with $\bar E^\top p \in \mathcal{N}_{u_2}$, since $\mathcal{Z} \subseteq \ker \bar E$ and $R(p)^\top = \bar E U(\bar E^\top p)$, we have

$$\ker G_{\mathcal{Z}}(p) = \{\xi \in \mathbb{R}^m : U(\bar E^\top p)\xi \in \mathcal{Z}\} \subseteq \ker R(p)^\top. \tag{16}$$

At any $p \in \mathcal{M}_{y_1}$ (so $\bar E^\top p \in \mathcal{C}$ and $\ell = 0$), Proposition 1 implies that $\dot\xi = 0$ if and only if $\xi \in \ker G_{\mathcal{Z}}(p)$, which by (16) also yields $\dot p = -b\,R(p)^\top \xi = 0$, with equilibrium edge forces $y_2 = b\,U(\bar E^\top p)\xi \in \mathcal{Z}$. Since $\ker R(p)^\top = \mathrm{diag}(d)\ker(R_{\mathcal{G}}(p)^\top)$ on $\mathcal{M}_{y_1}$ is the normalized self-stress space, the controller equilibria $\ker G_{\mathcal{Z}}(p)$ at $p \in \mathcal{M}_{y_1}$ are precisely the normalized self-stresses whose induced edge forces lie in $\mathcal{Z}$, with $\ker G_{\ker \bar E}(p) = \ker R(p)^\top$.

Moreover, for a held $p \in \mathcal{M}_{y_1}$, Σ_2 in (13) reduces to $\dot\xi = -a\,G_{\mathcal{Z}}(p)\xi$ with $e_{y_2} = b\,\mathrm{P}_{\mathcal{Z}^\perp} U(\bar E^\top p)\xi$. This shows the selective role of output-strict $(\mathcal{C}, \mathcal{Z})$-passivity: it leaves the equilibrium modes in $\ker G_{\mathcal{Z}}(p)$ unpenalized while exponentially damping the orthogonal modes in $(\ker G_{\mathcal{Z}}(p))^\perp$ and the off-target output error e_{y_2}.

In general, $G_{\mathcal{Z}}(p)$ depends on p through the edge directions. Rotating a configuration by $Q \in SO(2)$ maps $U(\bar E^\top p)$ to $(I_m \otimes Q)U(\bar E^\top p)$, so $G_{\mathcal{Z}}$ changes to $U(\bar E^\top p)^\top (I_m \otimes Q)^\top \mathrm{P}_{\mathcal{Z}^\perp}(I_m \otimes Q)U(\bar E^\top p)$, which coincides with $G_{\mathcal{Z}}(p)$ only if $\mathcal{Z}$ is rotation-invariant. Moreover, the convergence analysis requires the damped modes, i.e., the positive spectrum of $G_{\mathcal{Z}}(p)$, to remain uniformly damped near $\mathcal{M}_{y_1}$. We therefore impose the following assumption.

Assumption 1: The subspace $\mathcal{Z} \subseteq \ker \bar E$ satisfies:

i) *Rotation invariance:* $(I_m \otimes Q)\mathcal{Z} = \mathcal{Z}$ for all $Q \in SO(2)$;

ii) *Uniform spectral gap:* there exist $\rho > 0$ and $\mu_{\mathcal{Z}} \in (0, 1]$ such that on

$$\mathcal{T}_\rho := \{p \in \mathbb{R}^{2n} : \mathrm{dist}(p, \mathcal{M}_{y_1}) < \rho\} \subseteq \mathcal{N}_{y_1},$$

we have $\bar E^\top p \in \mathcal{N}_{u_2}$ and every positive eigenvalue of $G_{\mathcal{Z}}(p)$ lies in $[\mu_{\mathcal{Z}}, 1]$.

Assumption 1(i) holds for any $\mathcal{Z} = \mathcal{Z}_0 \otimes \mathbb{R}^2$ with $\mathcal{Z}_0 \subseteq \ker E$ (e.g., $\mathcal{Z} = \{0\}$ or $\ker \bar E = \ker E \otimes \mathbb{R}^2$). Under Assumption 1(i), $\mathrm{P}_{\mathcal{Z}^\perp}$ commutes with $I_m \otimes Q$, so $G_{\mathcal{Z}}(p)$ is invariant under planar rigid motions; in particular, $G_{\mathcal{Z}}(p) = G_{\mathcal{Z}}(p^\star)$ on $\mathcal{M}_{y_1}$, and the closed-loop equilibrium set on $\mathcal{M}_{y_1}$ is

$$\mathcal{X}_\star := \mathcal{M}_{y_1} \times \ker G_{\mathcal{Z}}(p^\star). \tag{17}$$

Since $\bar E^\top \mathcal{M}_{y_1} \subseteq \mathcal{C}$ and $\mathcal{Z} \subseteq \ker \bar E$, $\mathcal{X}_\star$ also coincides with the closed-loop feasible state set in the sense of [12], on which all four realized ports lie in $(\mathcal{M}_{u_1}, \mathcal{M}_{y_1}, \mathcal{C}, \mathcal{Z})$. Moreover, by this invariance, Assumption 1(ii) holds (for ρ sufficiently small) whenever $G_{\mathcal{Z}}(p)$ has constant rank near $p^\star$.

C. Available Dissipation and the Realized Margin

Along the closed-loop trajectories, the controller dissipation equality in (12) reads $\dot{V}_2 = \langle e_{u_2}, e_{y_2}\rangle - W_0(p,\xi)$, with

$$W_0(p,\xi) := a\,\xi^\top G_{\mathcal{Z}}(p)\xi + g\,\ell^\top G_{\mathcal{Z}}(p)\ell. \tag{18}$$

Following [12], we retain this exact available dissipation $W_0(p,\xi)$ rather than the more conservative bound $\frac{a}{b^2+ag}\|e_{y_2}\|^2$ in (12). We next characterize the channel compatibility of the interconnection in Fig. 1.

Proposition 2 (Channel compatibility): Consider the interconnection Fig. 1 with port targets (5), (6), and (8).

i) The reverse channel $-\bar{E}$ is exactly compatible on $\mathbb{R}^{2m}$.

ii) The forward channel $\bar{E}^\top$ has the defect

$$\begin{aligned}\delta_{\mathrm{fc}}(p) &= e_{u_2}(\bar{E}^\top p) - \bar{E}^\top e_{y_1}(p)\\ &= \bar{E}^\top r_{y_1}(p) - r_{u_2}(\bar{E}^\top p),\end{aligned} \tag{19}$$

which vanishes on $\mathcal{M}_{y_1}$. However, for $n \geq 3$, the forward channel is not first-order compatible along any nonempty subset of $\mathcal{M}_{y_1}$, and hence not exactly compatible on any neighborhood of a point of $\mathcal{M}_{y_1}$.

iii) For every $p \in \mathcal{N}_{y_1}$ with $\bar{E}^\top p \in \mathcal{N}_{u_2}$, the radial component of the forward defect is of second order:

$$\big\|U(\bar{E}^\top p)^\top \delta_{\mathrm{fc}}(p)\big\| \leq C\|e_{y_1}(p)\|^2, \tag{20}$$

with $C := 2\|\bar{E}\|^2/\min_k d_k$.

Proof: i) Since $\mathcal{M}_{u_1} = \{0\}$, we have $r_{u_1} \equiv 0$, and $\mathcal{Z} \subseteq \ker \bar{E}$ gives $\delta_{\mathrm{rc}}(y_2) = -\bar{E}\,\mathrm{P}_{\mathcal{Z}} y_2 - r_{u_1}(-\bar{E}y_2) = 0$ for all $y_2 \in \mathbb{R}^{2m}$.

ii) For $p \in \mathcal{M}_{y_1}$, we have $r_{y_1}(p) = p$ and $\bar{E}^\top p \in \mathcal{C}$, so $r_{u_2}(\bar{E}^\top p) = \bar{E}^\top p$ and $\delta_{\mathrm{fc}}(p) = 0$. At such p, the differentials of the nearest-point projections are the tangent-space projectors, so $\mathrm{d}_p\delta_{\mathrm{fc}} = \bar{E}^\top \mathrm{P}_{T_p\mathcal{M}_{y_1}} - \mathrm{P}_{T_{\bar{E}^\top p}\mathcal{C}}\,\bar{E}^\top$. Let J denote the rotation by $\pi/2$. Since $T_p\mathcal{M}_{y_1}$ is spanned by the translations, which lie in $\ker \bar{E}^\top$, and the infinitesimal rotation $(I_n \otimes J)p$, with $\bar{E}^\top(I_n \otimes J)p = (I_m \otimes J)\bar{E}^\top p \neq 0$, the first term has rank one. For the second term, $\mathrm{P}_{T_{\bar{E}^\top p}\mathcal{C}} = I_{2m} - UU^\top$ with $U = U(\bar{E}^\top p)$, so $v \in \ker(\mathrm{P}_{T_{\bar{E}^\top p}\mathcal{C}}\bar{E}^\top)$ if and only if each relative velocity $(\bar{E}^\top v)_k$ is parallel to $(\bar{E}^\top p)_k$, i.e., $R_{\mathcal{G}}(p)(I_n \otimes J)^\top v = 0$. By infinitesimal rigidity, this kernel is three-dimensional, so the second term has rank $2n - 3 \geq 3$. Hence, $\mathrm{d}_p\delta_{\mathrm{fc}} \neq 0$ for every $p \in \mathcal{M}_{y_1}$, and δ_{fc} cannot vanish identically near any such p.

iii) Fix an edge e_k and let $\bar{u}_k := (\bar{E}^\top r_{y_1}(p))_k$ denote the corresponding edge of the nearest target formation. Since $r_{y_1}(p) \in \mathcal{M}_{y_1}$, both $\bar{u}_k$ and $r_{u_2,k} = d_k\widehat{u}_{2,k}$ lie on the circle d_kS^1, and $\delta_{\mathrm{fc},k} = \bar{u}_k - d_k\widehat{u}_{2,k}$. Expanding the squared norm with $\|\bar{u}_k\| = d_k$ gives

$$\begin{aligned}\|\delta_{\mathrm{fc},k}\|^2 &= \|\bar{u}_k\|^2 - 2d_k\widehat{u}_{2,k}^\top\bar{u}_k + d_k^2\\ &= 2d_k\big(d_k - \widehat{u}_{2,k}^\top\bar{u}_k\big) = -2d_k\,\widehat{u}_{2,k}^\top\delta_{\mathrm{fc},k},\end{aligned}$$

so the radial component of each chord is quadratic in its length,

$$\big|\widehat{u}_{2,k}^\top\delta_{\mathrm{fc},k}\big| = \frac{\|\delta_{\mathrm{fc},k}\|^2}{2d_k}.$$

Next, since $\bar{E}^\top r_{y_1}(p) \in \bar{E}^\top\mathcal{M}_{y_1} \subseteq \mathcal{C}$, the nearest-point property of r_{u_2} gives

$$\begin{aligned}\|e_{u_2}(\bar{E}^\top p)\| &= \|\ell\| = \mathrm{dist}(\bar{E}^\top p, \mathcal{C})\\ &\leq \|\bar{E}^\top e_{y_1}(p)\| \leq \|\bar{E}\|\,\|e_{y_1}(p)\|,\end{aligned}$$

and hence, by (19),

$$\|\delta_{\mathrm{fc}}\| \leq \|e_{u_2}\| + \|\bar{E}^\top e_{y_1}\| \leq 2\|\bar{E}\|\,\|e_{y_1}\|.$$

Combining these bounds yields

$$\begin{aligned}\|U^\top\delta_{\mathrm{fc}}\| &\leq \sum_{k=1}^m \big|\widehat{u}_{2,k}^\top\delta_{\mathrm{fc},k}\big| = \sum_{k=1}^m \frac{\|\delta_{\mathrm{fc},k}\|^2}{2d_k}\\ &\leq \frac{\|\delta_{\mathrm{fc}}\|^2}{2\min_k d_k} \leq C\|e_{y_1}\|^2.\end{aligned}$$

■

By Proposition 2ii), the interconnection results of [12] for exactly or first-order compatible channels do not apply. Intuitively, the edgewise target $\mathcal{C}$ allows each edge to rotate independently on its own circle, whereas on $\bar{E}^\top\mathcal{M}_{y_1}$ all edges can only rotate together. Therefore, off $\mathcal{M}_{y_1}$, the two projections in (19) differ to first order, but only along the edge-rotation (tangential) directions. Item iii) is the structural property that nevertheless yields a dissipation margin: although δ_{fc} is of first order in general, the controller output (13) is radial, so δ_{fc} enters the energy balance only through its second-order radial component (cf. Fig. 2).

Since $\delta_{\mathrm{rc}} \equiv 0$ by Proposition 2 i), the composite storage $V_{\mathrm{cl}}(p,\xi) = V_1(p) + V_2(\xi) = \frac{1}{2}\|e_{y_1}(p)\|^2 + \frac{1}{2}\|\xi\|^2$ satisfies the closed-loop dissipation identity

$$\dot{V}_{\mathrm{cl}} = \langle\delta_{\mathrm{fc}}(p), e_{y_2}\rangle - W_0(p,\xi) =: s_\delta(p,\xi) - W_0(p,\xi). \tag{21}$$

Comparing s_δ with W_0 yields the following margin.

Lemma 1 (Dissipation margin): Under Assumption 1 with spectral bound $\mu_{\mathcal{Z}}$, if the controller gains satisfy

$$4ag\mu_{\mathcal{Z}} > b^2(1-\mu_{\mathcal{Z}})^2, \tag{22}$$

then there exist $r \in (0,\rho]$ and $\alpha > 0$ such that, for every $p \in \mathcal{T}_r$ and $\xi \in \mathbb{R}^m$,

$$\dot{V}_{\mathrm{cl}} \leq -\alpha\big(\|e_{y_1}(p)\|^2 + \xi^\top G_{\mathcal{Z}}(p)\xi\big). \tag{23}$$

Proof: For brevity, write $U = U(\bar{E}^\top p)$, $G = G_{\mathcal{Z}}(p)$, $R = R(p)$, $e = e_{y_1}(p)$, and $\delta = \delta_{\mathrm{fc}}(p)$, and define

$$X := \sqrt{\xi^\top G\xi},\ Y := \|Re\|.$$

Step 1 (energy balance). Since $e_{u_2} = U\ell$, we have $\delta = U\ell - \bar{E}^\top e$, and $U^\top U = I_m$ with $R = U^\top\bar{E}^\top$ gives

$$\ell = Re + U^\top\delta.$$

Moreover, $e_{y_2} = \mathrm{P}_{\mathcal{Z}^\perp}U(b\xi + g\ell)$ and $\bar{E}\,\mathrm{P}_{\mathcal{Z}} = 0$ give

$$\begin{aligned}\langle U\ell, e_{y_2}\rangle &= \ell^\top G(b\xi + g\ell)\\ \langle\bar{E}^\top e, e_{y_2}\rangle &= (Re)^\top(b\xi + g\ell).\end{aligned}$$

Substituting these relations into (21) yields

$$\begin{aligned}\dot{V}_{\mathrm{cl}} = &-a\,\xi^\top G\xi - g\|Re\|^2 - b(Re)^\top(I_m - G)\xi\\ &- (U^\top\delta)^\top\big(g\,Re - b\,G\xi\big).\end{aligned} \tag{24}$$

Step 2 (quadratic terms). By (16), every $\zeta \in \ker G$ satisfies $U\zeta \in \mathcal{Z} \subseteq \ker \bar{E}$, so $\zeta^\top Re = (\bar{E}U\zeta)^\top e = 0$, i.e., $Re \perp \ker G$. Since the positive eigenvalues of G lie in $[\mu_{\mathcal{Z}}, 1]$ by Assumption 1(ii), it follows that

$$\big|(Re)^\top (I_m - G)\xi\big| \le \frac{1-\mu_{\mathcal{Z}}}{\sqrt{\mu_{\mathcal{Z}}}}\, XY.$$

Hence, the first three terms in (24) are bounded by the quadratic form $-aX^2 - gY^2 + b\frac{1-\mu_{\mathcal{Z}}}{\sqrt{\mu_{\mathcal{Z}}}} XY$, which is negative definite under (22). Thus, there exists $\alpha_0 > 0$ such that

$$-aX^2 - gY^2 - b(Re)^\top (I_m - G)\xi \le -2\alpha_0 (X^2 + Y^2).$$

Step 3 (lower bound on Y). Since $e \in N_{r_{y_1}(p)}\mathcal{M}_{y_1} = (\ker R(r_{y_1}(p)))^\perp$, infinitesimal rigidity and the invariance of $\mathcal{M}_{y_1}$ under planar rigid motions give a constant $\sigma_\star > 0$ such that $\|R(r_{y_1}(p))e\| \ge \sigma_\star \|e\|$. Since $R(p)e = R(r_{y_1}(p))e + O(\|e\|^2)$, there exist $r \in (0, \rho]$ and $c_1 > 0$ such that

$$Y \ge c_1 \|e\| \qquad \text{for all } p \in \mathcal{T}_r.$$

Step 4 (remainder). By Proposition 2iii), $\|U^\top \delta\| \le C\|e\|^2$. Together with $\|G\xi\| \le X$, which follows from $0 \preceq G \preceq I_m$, and Step 3, the last term in (24) satisfies

$$\begin{aligned}\big|(U^\top \delta)^\top (g\, Re - b\, G\xi)\big| &\le C\|e\|^2 (gY + bX) \\ &\le C'\|e\| \left(X^2 + Y^2\right),\end{aligned}$$

with $C' := C(2g + b)/(2c_1)$. Shrinking r so that $C'r \le \alpha_0$ and combining Steps 1–4 yields $\dot{V}_{\mathrm{cl}} \le -\alpha_0 (X^2 + Y^2)$ on $\mathcal{T}_r$. By Step 3, this implies (23) with $\alpha := \alpha_0 \min\{1, c_1^2\}$. ∎

Remark 1 (Role of the gain condition): For $\mathcal{Z} \neq \{0\}$, the residual supply s_δ in (21) retains a nonzero quadratic part near $\mathcal{X}_\star$. Indeed, at any $(\bar{p}, 0)$ with $\bar{p} \in \mathcal{M}_{y_1}$, writing $\bar{R} := R(\bar{p})$ and $\bar{G} := G_{\mathcal{Z}}(\bar{p})$, a state perturbation (v, η) yields

$$s_\delta(\bar{p} + tv,\, t\eta) = -t^2 (\bar{R}v)^\top (I_m - \bar{G})(b\,\eta + g\bar{R}v) + O(t^3),$$

whose quadratic part is nonzero whenever $\bar{R}^\top (I_m - \bar{G}) \neq 0$. The closed loop thus falls into the *nonzero quadratic residual* case of the compatibility hierarchy in [12], so part of the available dissipation W_0 must be spent to dominate s_δ; this is the origin of the gain condition (22). For $\mathcal{Z} = \{0\}$, we have $\bar{G} = I_m$ and the quadratic part cancels (*quadratic cancellation*), consistent with Corollary 1 holding for all gains $a, b, g > 0$.

D. Compact Confinement and Convergence

Fixing $r \in (0, \rho]$ from Lemma 1, we define the *closed-loop analysis domain* $\mathcal{D} := \mathcal{T}_r \times \mathbb{R}^m$, on which (23) holds. However, Lemma 1 alone does not guarantee convergence: (23) holds only locally and leaves planar translations along $\mathcal{M}_{y_1}$ and modes in $\ker G_{\mathcal{Z}}(p)$ unpenalized, rendering the sublevel sets of V_{cl} noncompact. We next combine these sublevel sets with the conserved formation centroid to obtain compact confinement and closed-loop convergence.

Theorem 1 (Local state-set and port convergence): Consider the closed loop of Σ_1 and Σ_2 interconnected via Fig. 1. Suppose Assumption 1 and the gain condition (22) hold. Then, there exists $\varepsilon_0 > 0$ such that every solution with $(p(0), \xi(0)) \in \mathcal{D}$ and $V_{\mathrm{cl}}(p(0), \xi(0)) < \varepsilon_0$ is forward complete, remains in a compact subset of $\mathcal{D}$, and satisfies

$$\lim_{t\to\infty} \operatorname{dist}\big((p(t), \xi(t)), \mathcal{X}_\star\big) = 0. \tag{25}$$

Moreover, the port signals u_1, y_1, u_2, and y_2 converge to $\mathcal{M}_{u_1}$, $\mathcal{M}_{y_1}$, $\mathcal{C}$, and $\mathcal{Z}$, respectively.

Proof: Choose $\varepsilon_0 \in (0, r^2/2)$ and let $c := V_{\mathrm{cl}}(p(0), \xi(0)) < \varepsilon_0$. Since $(\mathbf{1}_n^\top \otimes I_2)\bar{E} = 0$, the centroid $\chi(p) := (\mathbf{1}_n^\top \otimes I_2)p$, with $\dot{\chi} = 0$, is conserved. On $\{V_{\mathrm{cl}} \le c\}$, we have $\operatorname{dist}(p, \mathcal{M}_{y_1}) = \|e_{y_1}(p)\| \le \sqrt{2c} < r$ and $\|\xi\| \le \sqrt{2c}$. Since $\mathcal{M}_{y_1}$ is translation-invariant, $r_{y_1}(p)$ preserves χ, so fixing $\chi(p) = \chi(p(0))$ restricts $r_{y_1}(p)$ to a compact $SO(2)$-orbit. Thus, $\Omega_c := \{(p, \xi) \in \mathcal{D} : V_{\mathrm{cl}}(p, \xi) \le c,\ \chi(p) = \chi(p(0))\}$ is a compact subset of $\mathcal{D}$. Moreover, Ω_c is forward invariant: as long as $p(t) \in \mathcal{T}_r$, (23) gives $\dot{V}_{\mathrm{cl}} \le 0$, so $\operatorname{dist}(p(t), \mathcal{M}_{y_1}) \le \sqrt{2c} < r$ and the trajectory cannot reach the boundary of $\mathcal{T}_r$. This ensures forward completeness and compact confinement by [12, Proposition 6]. Next, since $\|e_{u_2}(\bar{E}^\top p)\| = \|\ell\| \le \|\bar{E}\| \|e_{y_1}(p)\|$ from the proof of Proposition 2 iii), it follows from (13) that

$$\|e_{y_2}(y_2)\| \le b\sqrt{\xi^\top G_{\mathcal{Z}}(p)\xi} + g\|\ell\|,\ \ \|u_1\| \le \|\bar{E}\| \|e_{y_2}(y_2)\|, \tag{26}$$

and, since the squared distance to a product set is the sum of the squared distances to its factors, $\operatorname{dist}\big((p, y_2), \mathcal{M}_{y_1} \times \mathcal{Z}\big)^2 = \|e_{y_1}(p)\|^2 + \|e_{y_2}(y_2)\|^2 \le (1 + 2g^2\|\bar{E}\|^2)\|e_{y_1}(p)\|^2 + 2b^2 \xi^\top G_{\mathcal{Z}}(p)\xi$. Hence, (23) satisfies the port-distance margin of [12, Theorem 2], yielding $(p, y_2) \to \mathcal{M}_{y_1} \times \mathcal{Z}$ and, by (26), $(u_1, u_2) \to \mathcal{M}_{u_1} \times \mathcal{C}$. Finally, $\ell \to 0$ and $e_{y_2} = \mathrm{P}_{\mathcal{Z}^\perp} U(b\xi + g\ell) \to 0$ imply $\xi^\top G_{\mathcal{Z}}(p)\xi = \|\mathrm{P}_{\mathcal{Z}^\perp} U\xi\|^2 \to 0$. Hence, every accumulation point $(\bar{p}, \bar{\xi}) \in \Omega_c$ of the trajectory satisfies $\bar{p} \in \mathcal{M}_{y_1}$ and $\bar{\xi} \in \ker G_{\mathcal{Z}}(\bar{p}) = \ker G_{\mathcal{Z}}(p^\star)$, i.e., lies in $\mathcal{X}_\star$ by (17), and compactness of Ω_c yields (25). ∎

We next specialize Theorem 1 to $\mathcal{Z} = \{0\}$. In this case, $\mathrm{P}_{\mathcal{Z}^\perp} = I_{2m}$, so that the controller (13) decouples across edges into $\dot{\xi}_k = b\ell_k - a\xi_k$ and $y_{2,k} = \widehat{u}_{2,k}(b\xi_k + g\ell_k)$ for $k \in \{1, \dots, m\}$, and the target equilibrium set reduces to $\mathcal{X}_\star = \mathcal{M}_{y_1} \times \{0\}$.

Corollary 1 (Independent edge controllers): Consider the closed loop of Σ_1 and Σ_2 interconnected via Fig. 1 with $\mathcal{Z} = \{0\}$ and any $a, b, g > 0$. Then there exists $\varepsilon_0 > 0$ such that every solution with $(p(0), \xi(0)) \in \mathcal{D}$ and $V_{\mathrm{cl}}(p(0), \xi(0)) < \varepsilon_0$ converges exponentially to $\mathcal{M}_{y_1} \times \{0\}$, and $p(t)$ converges to a single configuration in $\mathcal{M}_{y_1}$.

Proof: When $\mathcal{Z} = \{0\}$, we have $G_{\mathcal{Z}}(p) = I_m$ and $\mu_{\mathcal{Z}} = 1$, so Assumption 1 and (22) hold for all $a, b, g > 0$. By Theorem 1, for $\varepsilon_0 \in (0, r^2/2)$, every solution with $V_{\mathrm{cl}}(0) < \varepsilon_0$ remains in $\mathcal{D}$ for all $t \ge 0$, where (23) reduces to $\dot{V}_{\mathrm{cl}} \le -2\alpha V_{\mathrm{cl}}$. Consequently, $V_{\mathrm{cl}}(t) \le V_{\mathrm{cl}}(0) e^{-2\alpha t}$ and $\operatorname{dist}\big((p(t), \xi(t)), \mathcal{M}_{y_1} \times \{0\}\big) = \sqrt{2V_{\mathrm{cl}}(t)} \le \sqrt{2V_{\mathrm{cl}}(0)}\, e^{-\alpha t}$, establishing exponential convergence to $\mathcal{M}_{y_1} \times \{0\}$. Moreover, by (26), $\|\dot{p}(t)\| = \|u_1(t)\| \le C\sqrt{2V_{\mathrm{cl}}(t)} \le C\sqrt{2V_{\mathrm{cl}}(0)}\, e^{-\alpha t}$ for some $C > 0$, which is integrable on $[0, \infty)$. Thus, $p(t)$ converges to a single configuration in $\mathcal{M}_{y_1}$. ∎

While $\mathcal{Z} = \{0\}$ in Corollary 1 eliminates inter-edge coupling with $\mu_{\{0\}} = 1$, it sustains no nonzero equilibrium

forces. At the other extreme, $\mathcal{Z} = \ker \bar{E}$ retains the full self-stress space $\ker R(p^\star)^\top$, but its projector $\mathrm{P}_{(\ker \bar{E})^\perp}$ is generally dense and couples nonadjacent edges. Whenever a smaller subspace $\mathcal{Z} \subsetneq \ker \bar{E}$ has the same intersection with $\operatorname{range} U(\bar{E}^\top p)$ as $\ker \bar{E}$ near $\mathcal{M}_{y_1}$, we have $G_{\mathcal{Z}}(p) \succeq G_{\ker \bar{E}}(p)$ with the same kernel $\ker R(p)^\top$, which preserves the admissible equilibrium forces and admits $\mu_{\mathcal{Z}} \geq \mu_{\ker \bar{E}}$. In particular, when the desired equilibrium forces are supported on a local subgraph, choosing $\mathcal{Z}$ as the subspace of balanced forces supported on that subgraph confines the coupling of $\mathrm{P}_{\mathcal{Z}^\perp}$ to the subgraph and decouples the remaining edges, as illustrated in Section V.

V. Numerical results

We illustrate three aspects of the results: how the output target $\mathcal{Z}$ selects equilibrium edge forces sustained at steady state, the second-order scaling of the forward compatibility defect in Proposition 2, and the role of the spectral bound $\mu_{\mathcal{Z}}$ in the convergence rate.

Consider $n = 12$ agents with target positions $p_i^\star = (0.9(i-1), y_i)$, where $(y_1, \dots, y_{12}) = (0, 1.2, -0.7, 1.3, 0, 1.1, -0.2, 1.2, 0.2, 1.9, -0.2, 1.2)$. The edges $\{i, i+1\}$ and $\{i, i+2\}$ form a chain of triangles, to which we add the two long-range links $\{1, 5\}$ and $\{8, 12\}$, giving $m = 23$ edges (Fig. 3(a)). The framework is infinitesimally rigid, and each long-range link creates one independent self-stress: one is nonzero exactly on the eight edges among agents 1–5, the other on the eight edges among agents 8–12, and the seven edges in between carry no self-stress.

We split the agents into a left group $L = \{1, \dots, 6\}$ and a right group $R = \{7, \dots, 12\}$ and compare five output targets:

- $\mathcal{Z} = \{0\}$: no nonzero equilibrium force is retained;
- $\mathcal{Z}_L$: the balanced edge forces in $\ker \bar{E}$ that vanish on every edge not joining two agents of L;
- $\mathcal{Z}_R$: defined analogously for R;
- $\mathcal{Z}_L \oplus \mathcal{Z}_R$: the sum of the two;
- $\mathcal{Z} = \ker \bar{E}$: all balanced edge forces.

Each target has the form $\mathcal{Z}_0 \otimes \mathbb{R}^2$ and thus satisfies Assumption 1(i), and $\dim \ker G_{\mathcal{Z}}(p(t))$ stays constant along all simulated trajectories, consistent with Assumption 1(ii). We use $a = b = 1$ and $g = 25$, which satisfy (22) at $\mu_{\mathcal{Z}}(p^\star)$ for every target. Each target is simulated from the initial condition of Fig. 3(a) and from 20 random ones, in which $p(0)$ is a randomly rotated and translated copy of $p^\star$ perturbed by Gaussian noise with standard deviation 0.25, and $\xi(0)$ is random.

Sustained equilibrium forces. In all runs, the formation converges to the target shape and $\xi(t)$ converges to a normalized self-stress $\xi_\infty \in \ker G_{\mathcal{Z}}(p^\star)$, inducing edge forces that balance at every agent. The output target determines which edges carry these forces (Fig. 3(a)): under $\mathcal{Z}_L$, only the eight edges among agents 1–5 remain stressed, whereas under $\mathcal{Z}_L \oplus \mathcal{Z}_R$ and $\ker \bar{E}$, both groups of eight edges are stressed. Which edges are stressed is the same in every run of a given design; only the magnitude of ξ_∞ depends on the initial condition. The stressed edges also have a simple interpretation: an edge can carry a nonzero equilibrium force exactly when it is redundant, i.e., when removing it preserves infinitesimal rigidity [13], [14]. For example, the links $\{4, 6\}$ and $\{5, 6\}$ remain unstressed under $\mathcal{Z}_L$, and removing either of them makes the formation flexible.

Forward compatibility defect. Fig. 4(b) checks Proposition 2 at configurations displaced from $p^\star$ in 40 random directions normal to $\mathcal{M}_{y_1}$, and along the closed-loop trajectory for $\mathcal{Z}_L$. The full defect δ_{fc} grows linearly with the distance to the target (fitted slope 1.00), so the forward channel is not first-order compatible. Its radial component $U^\top \delta_{\mathrm{fc}}$, which is the only part that enters the closed-loop energy balance (24), grows quadratically (fitted slope 2.00) and remains below the bound (20) with $C = 9.94$.

Spectral bound and convergence rate. Fig. 3(b) and Fig. 4(a) show that convergence slows down as $\mu_{\mathcal{Z}}$ decreases. To test this relation beyond the five designs, Fig. 4(c) plots the slowest decay rate of the closed loop, linearized at $(p^\star, 0)$, against $\mu_{\mathcal{Z}}$ for 50 output targets: the five above, and the targets obtained in the same way as $\mathcal{Z}_L$ from every group of four or more consecutive agents. For $g = 25$, the rate matches $(a + b^2/g)\,\mu_{\mathcal{Z}}$ within 0.5% for every target except $\mathcal{Z} = \{0\}$: the agents settle quickly, and the controller states then decay at a rate set by $\mu_{\mathcal{Z}}$. For $g = 2$, the rate follows $\mu_{\mathcal{Z}}$ until the agent dynamics become the bottleneck. The output target thus trades the sustained equilibrium forces against coupling and speed: $\mathcal{Z}_L \oplus \mathcal{Z}_R$ and $\ker \bar{E}$ sustain the same equilibrium forces, but $\ker \bar{E}$ couples all 253 edge pairs instead of 90, has a seven times smaller $\mu_{\mathcal{Z}}$, and settles about seven times more slowly.

VI. Concluding remarks

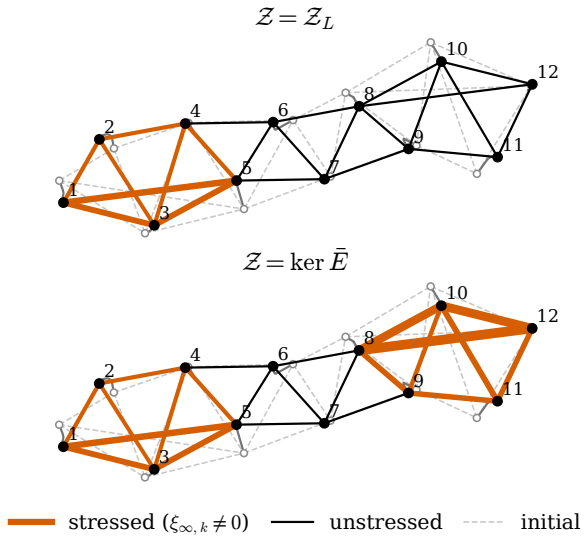
We develop a passivity-based dynamical synthesis for distance-constrained formations using transversal passivity. By encoding the desired formation geometry and balanced edge forces as port target manifolds, the control task is reformulated as the joint design of a transversally passive edge controller and its output-target subspace. We propose a constructive realization of an output-strictly transversally passive edge controller that sustains the corresponding equilibrium edge forces, and establish a closed-loop dissipation margin and local convergence to the target manifolds. While sustaining nonzero equilibrium forces generally leads to a centralized implementation, numerical simulations illustrate how a localized output-target subspace can preserve these forces with sparser coupling. Future work will explore sparse output-target designs for distributed controller implementation and develop a general synthesis framework for transversal passivity.

References

[1] B. D. O. Anderson, C. Yu, B. Fidan, and J. M. Hendrickx, "Rigid graph control architectures for autonomous formations," *IEEE Control Systems Magazine*, vol. 28, no. 6, pp. 48–63, 2008.

[2] K.-K. Oh, M.-C. Park, and H.-S. Ahn, "A survey of multi-agent formation control," *Automatica*, vol. 53, pp. 424–440, 2015.

[3] R. Babazadeh and R. Selmic, "Distance-based multiagent formation control with energy constraints using sdre," *IEEE Transactions on Aerospace and Electronic Systems*, vol. 56, no. 1, pp. 41–56, 2019.



(a)

$\mathcal{Z}$	stressed	coupled pairs	$\mu_{\mathcal{Z}}$	local rate	t_s (med./max)
$\{0\}$	0	0	1.000	0.877	5.5 / 7.1
$\mathcal{Z}_L$	8	45	0.131	0.136	21.6 / 28.0
$\mathcal{Z}_R$	8	45	0.078	0.082	35.9 / 49.9
$\mathcal{Z}_L \oplus \mathcal{Z}_R$	16	90	0.078	0.082	36.2 / 49.9
$\ker \bar{E}$	16	253	0.011	0.012	248.9 / 368.9

(b)

Fig. 3: (a) Agent trajectories (gray) from the initial (dashed) to the final formation for $\mathcal{Z} = \mathcal{Z}_L$ (top) and $\mathcal{Z} = \ker \bar{E}$ (bottom); highlighted edges carry a nonzero sustained stress $\xi_{\infty,k}$, with line width proportional to $|\xi_{\infty,k}|$. (b) For each output target: number of stressed edges, edge pairs coupled by $\mathrm{P}_{\mathcal{Z}^\perp}$, spectral bound $\mu_{\mathcal{Z}}$ at $p^\star$, slowest local decay rate at $(p^\star, 0)$, and settling time t_s of $\|\ell(t)\| \leq 10^{-3}$ (median and maximum over 20 random initial conditions), for $a = b = 1$ and $g = 25$.

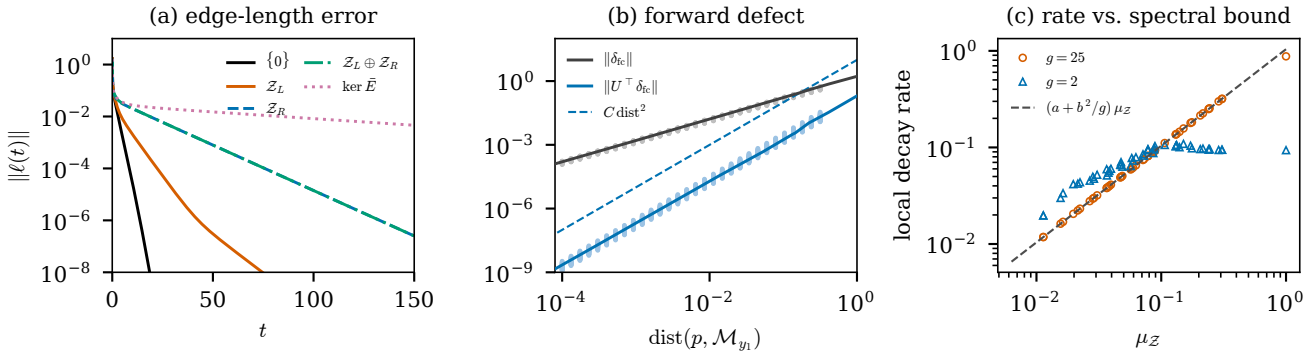


Fig. 4: (a) Edge-length error $\|\ell(t)\| = \|e_{u_2}(u_2(t))\|$ from the initial condition of Fig. 3(a); the curves for $\mathcal{Z}_R$ and $\mathcal{Z}_L \oplus \mathcal{Z}_R$ nearly coincide. (b) Forward compatibility defect versus $\mathrm{dist}(p, \mathcal{M}_{y_1})$ at sampled configurations (dots) and along the closed-loop trajectory for $\mathcal{Z}_L$ (solid). (c) Slowest local decay rate versus $\mu_{\mathcal{Z}}$ for 50 output targets.

[4] L. Asimow and B. Roth, "The rigidity of graphs, II," *Journal of Mathematical Analysis and Applications*, vol. 68, no. 1, pp. 171–190, 1979.

[5] L. Krick, M. E. Broucke, and B. A. Francis, "Stabilisation of infinitesimally rigid formations of multi-robot networks," *International Journal of control*, vol. 82, no. 3, pp. 423–439, 2009.

[6] M. Arcak, "Passivity as a design tool for group coordination," *IEEE Transactions on Automatic Control*, vol. 52, no. 8, pp. 1380–1390, 2007.

[7] M. Sharf and D. Zelazo, "A network optimization approach to cooperative control synthesis," *IEEE Control Systems Letters*, vol. 1, no. 1, pp. 86–91, July 2017.

[8] N. Li, Z. Sun, A. van der Schaft, and J. M. Scherpen, "A port-hamiltonian framework for displacement-based and rigid formation tracking," *Automatica*, vol. 177, p. 112350, 2025.

[9] L. Theran, D. Zelazo, S. Dewar, and B. Schulze, "Formation control from the generic combinatorial viewpoint: edge dynamics and directed sensing," *arXiv preprint arXiv:2609.13423*, 2026.

[10] R. Connelly and W. Whiteley, "Second-order rigidity and prestress stability for tensegrity frameworks," *SIAM Journal on Discrete Mathematics*, vol. 9, no. 3, pp. 453–491, 1996.

[11] M. Tognon, C. Gabellieri, L. Pallottino, and A. Franchi, "Aerial co-manipulation with cables: The role of internal force for equilibria, stability, and passivity," *IEEE Robotics and Automation Letters*, vol. 3, no. 3, pp. 2577–2583, 2018.

[12] F.-Y. Yue and D. Zelazo, "Transversal passivity: Dissipation relative to input and output manifolds," 2026, arXiv:2611.06251. [Online]. Available: https://arxiv.org/abs/2611.06251

[13] L. Asimow and B. Roth, "The rigidity of graphs," *Transactions of the American Mathematical Society*, vol. 245, pp. 279–289, 1978.

[14] R. Connelly and S. D. Guest, *Frameworks, Tensegrities, and Symmetry*. Cambridge University Press, 2022.

[15] G. Laman, "On graphs and rigidity of plane skeletal structures," *Journal of Engineering mathematics*, vol. 4, no. 4, pp. 331–340, 1970.

[16] J. M. Lee, *Introduction to Smooth Manifolds*. Springer, 2003.

[17] A. van der Schaft and D. Jeltsema, "Port-Hamiltonian systems theory: An introductory overview," *Foundations and Trends in Systems and Control*, vol. 1, no. 2–3, pp. 173–378, 2014.

[18] A. van der Schaft, *L_2-Gain and Passivity Techniques in Nonlinear Control*, 3rd ed. Springer, 2017.